

# RSC Advances



This is an *Accepted Manuscript*, which has been through the Royal Society of Chemistry peer review process and has been accepted for publication.

*Accepted Manuscripts* are published online shortly after acceptance, before technical editing, formatting and proof reading. Using this free service, authors can make their results available to the community, in citable form, before we publish the edited article. This *Accepted Manuscript* will be replaced by the edited, formatted and paginated article as soon as this is available.

You can find more information about *Accepted Manuscripts* in the [Information for Authors](#).

Please note that technical editing may introduce minor changes to the text and/or graphics, which may alter content. The journal's standard [Terms & Conditions](#) and the [Ethical guidelines](#) still apply. In no event shall the Royal Society of Chemistry be held responsible for any errors or omissions in this *Accepted Manuscript* or any consequences arising from the use of any information it contains.

## ARTICLE

# Heteropolytungstic Acids Incorporated in Ordered Mesoporous Zirconia Framework as Efficient Oxidation Catalysts†

Cite this: DOI: 10.1039/x0xx00000x

Euaggelia Skliri,<sup>a</sup> Ioannis N. Lykakis<sup>b</sup> and Gerasimos S. Armatas<sup>\*a</sup>Received 00th January 2012,  
Accepted 00th January 2012

DOI: 10.1039/x0xx00000x

www.rsc.org/

Ordered mesoporous composite catalysts consisting of nanocrystalline tetragonal ZrO<sub>2</sub> and heteropolytungstic clusters, *i.e.* 12-phosphotungstic (PTA) and 12-silicotungstic (STA) acids, were prepared *via* a surfactant-assisted co-polymerization route. According to the X-ray diffraction, transmission electron microscopy and N<sub>2</sub> physisorption measurements, the resultant materials possess a well-defined mesoscopic order ranging from wormhole to hexagonal pore structure and exhibit large internal surface area (126–229 m<sup>2</sup>g<sup>-1</sup>) and quite narrow pore size distribution (*ca.* 2.2–2.6 nm in diameter). Energy dispersive X-ray microanalysis and infrared spectroscopy confirms that the heteropoly clusters are well dispersed within the zirconia matrix, while preserving intact their Keggin structure. The inclusion of PTA and STA clusters in mesoporous framework has a beneficial effect on the catalytic activity of these materials. Although zirconium oxide and heteropoly acids alone show little catalytic activity, the ZrO<sub>2</sub>–PTA and ZrO<sub>2</sub>–STA heterostructures exhibit surprisingly high activity in hydrogen peroxide mediated oxidation of 1,1-diphenyl-2-methyl propene under mild conditions. Indeed, the mesoporous ZrO<sub>2</sub>–STA composite sample loaded with 5 wt% STA shows a conversion rate 17 times higher than the mesoporous ZrO<sub>2</sub>. The catalytic activity of these materials is related to the spatial distribution of heteropoly acids in zirconia matrix and possible synergistic interactions between the incorporated Keggin units and Zr(IV) oxohydroxide species.

## Introduction

Polyoxometalates (POMs) are attractive metal-oxygen compounds of the early transition metals (V, Nb, Mo, W) with diverse molecular structures and adjustable functionality. These nanomaterials exhibit interesting physical properties such as strong Brønsted acidity, fast and reversible multi-stage redox activity and high thermal and hydrolytic stability, making them suitable for catalytic applications.<sup>1</sup> As a result, POMs have been extensively investigated as catalysts in a variety of chemical transformations and redox reactions. Examples include oxidative hydration and esterification of olefins, oxidation of alcohols<sup>2</sup> and alkenes<sup>3</sup>, and alkylation and acylation of hydrocarbons<sup>4</sup>.

Over the past few years, extensive research efforts have been made to immobilize POMs on a high-surface-area solid support as an efficient strategy for achieving high catalytic activity and reusability.<sup>5</sup> Compared to bulk heteropoly acids, supported POM clusters have various advantages, which are their large surface area, good accessibility to the reactants, and easier separation from the reaction mixture.<sup>6</sup> In addition, the

metal oxide surfaces could have a beneficial effect in catalytic processes through complementary or synergistic interactions with the POM compounds. For example, recently we indicated that incorporation of [PW<sub>12</sub>O<sub>40</sub>]<sup>3-</sup> Keggin clusters into the cobalt oxide matrix can dramatically improve the catalytic activity of mesoporous Co<sub>3</sub>O<sub>4</sub> towards N<sub>2</sub>O decomposition.<sup>7</sup> Therefore, the synthesis of high-surface-area mesoporous materials that combine the catalytic activity of POMs with the redox activity and durability of metal oxides is a major direction in catalysis research.

Impregnation is one of the most attractive synthetic routes towards mesoporous POM-based materials. This approach involves infiltration of soluble POM compounds within the pore channels of a previously synthesized host material, such as silica<sup>8</sup>, alumina<sup>9</sup>, titania and zirconia<sup>10</sup>. Although this is a simple yet efficient method, the impregnation process is often plagued by poor dispersion of POM units and pore blocking effects of the inorganic support. In addition, the impregnated POM clusters show moderately low chemical stability when anchored on surfaces with strong basic character (*e.g.* Al<sub>2</sub>O<sub>3</sub>,

MgO)<sup>11</sup>, while they are prone to leaching in polar solvents when anchored on weak acid or neutral supports (*e.g.* SiO<sub>2</sub>)<sup>12</sup>. Nevertheless, both the unprecedented molecular transport through nanopores and high hydrolytic stability of mesophase are valuable prerequisites for heterogeneous catalysis. A promising synthetic strategy to this end is the sol-gel inclusion of POMs in the pore walls of a mesoporous metal oxide material. This approach entails cross-linking polymerization of metal oxide and POM compounds in the presence of surfactants and allows controlled synthesis of mesoporous heterostructures with modulated POM/metal-oxide composition. Unlike to the impregnated analogues, the POM compounds in these materials constitute an integral part of the inorganic framework, forming rather a solid-solution structure.<sup>13</sup> Because of the excellent catalytic properties of POM clusters and the large pore surface of the host structure, mesoporous solids of this type are anticipated to have interesting perspectives in the applications as catalysts, exhibiting high activity and reusability.<sup>14</sup> While silica-based POM composites are easy to realize<sup>15</sup>, the synthesis of mesoporous heterostructures from transition-metal oxide and POM compounds still remains a challenge. The assembly of such complex materials requires an adjustment of the interaction between heteropoly acids and organic templates. Otherwise disordered mesophases of organic-inorganic aggregates due to the strong binding of heteropoly anions to the surfactant micelles might be formed.<sup>16</sup> Therefore, specific reaction conditions according to the choice of metal sources, template molecules, and POM anions are essential in order to achieve ordered POM-based mesoporous frameworks.

Zirconia (ZrO<sub>2</sub>) is an important n-type semiconductor material with great potential applications in redox and acid catalysis.<sup>17</sup> Recently, we demonstrated that well-ordered mesoporous frameworks consisting of nanocrystalline ZrO<sub>2</sub> and Keggin-type H<sub>3</sub>PMo<sub>12</sub>O<sub>40</sub> acids can be prepared *via* a soft-templating chemistry.<sup>18</sup> This work used non-ionic surfactant Pluronic P123 to direct the formation of hexagonal mesoporous ZrO<sub>2</sub>-based structures. These materials showed remarkable catalytic activity in H<sub>2</sub>O<sub>2</sub>-mediated oxidation of selected alkenes, which is comparable to that of homogeneous 12-phosphomolybdic acids. Herein, we report on the synthesis of a new type of mesoporous composite materials consisting of zirconium oxide and 12-phosphotungstic (H<sub>3</sub>PW<sub>12</sub>O<sub>40</sub>, PTA) or 12-silicotungstic (H<sub>4</sub>SiW<sub>12</sub>O<sub>40</sub>, STA) acid components. To produce these ZrO<sub>2</sub>-POM composites with different loading of POM clusters (*i.e.* ranging from 2 to 20 wt%), we utilized evaporation-induced cooperative self-assembly of Zr(IV) oxide dichloride and heteropoly tungstic acid compounds in the presence of the non-ionic surfactant polyoxoethylene cetyl ether (Brij-58) as structure-directing agent. The products possess a ZrO<sub>2</sub>-PTA and ZrO<sub>2</sub>-STA solid-solution structure with large and accessible surface area and narrow pore size distribution. More important, we also show that, although mesoporous zirconia and POM compounds alone have little catalytic activity, the ZrO<sub>2</sub>-POM composite frameworks exhibit surprisingly high activity in oxidation of 1,1-diphenyl-2-methyl propene under mild conditions. Indeed, the ZrO<sub>2</sub>-

STA sample loaded with 5 wt% STA is about 17 times more active than pure mesoporous ZrO<sub>2</sub>, while 12-silicotungstic acid alone shows negligible activity under similar conditions.

## Experimental

### Materials

12-Phosphotungstic acid (PTA) and 12-silicotungstic acid (STA) were purchased from Alfa Aesar. The solids were thermal treated at 100 °C for 2h in air to eliminate excess of uncoordinated water molecules. The weight proportion of water on dried samples was determined by TGA analysis (Perkin Elmer Diamond), obtaining a molecular formula of H<sub>3</sub>PW<sub>12</sub>O<sub>40</sub>·16H<sub>2</sub>O and H<sub>4</sub>SiW<sub>12</sub>O<sub>40</sub>·15H<sub>2</sub>O, respectively. Block copolymer surfactant (HO(CH<sub>2</sub>CH<sub>2</sub>O)<sub>20</sub>C<sub>16</sub>H<sub>33</sub>, M<sub>n</sub>~1124) designated as Brij-58, zirconium oxide dichloride (ZrOCl<sub>2</sub>·8H<sub>2</sub>O), absolute ethanol (99.8%) were purchased from Sigma-Aldrich and used with no further purification. The alkene used as substrate was synthesized based on literature procedure.<sup>19</sup>

### Synthesis of mesoporous ZrPTA and ZrSTA composites

Mesoporous zirconia and ZrO<sub>2</sub>-PTA and ZrO<sub>2</sub>-STA composite materials were prepared as following: In a typical preparation, 2 g of Brij-58 was dissolved in 20 mL of ethanol, forming a clear solution. Then, 3.2 g (10 mmol) of ZrOCl<sub>2</sub>·8H<sub>2</sub>O was added to the surfactant solution and the mixture was stirred vigorously for ~3 h at room temperature. After this, an appropriate amount of PTA or STA acids dissolved in 2 mL of ethanol was added slowly to the surfactant solution and the mixture was kept stirring for another 15 min. This solution was then poured into a Petri dish and left under static conditions at 40 °C for 3-4 days. The resulting solid product was subsequently dried at 100 °C under vacuum for 12 h. Template was removed by calcination in air at 265 °C with a heating rate of 0.5 °C min<sup>-1</sup> and held for 4 h and, then, at 350 °C with a heating rate of 0.5 °C min<sup>-1</sup> and held for 6 h. A series of mesoporous ZrO<sub>2</sub>-PTA (denoted as ZrPTA(*w*)) and ZrO<sub>2</sub>-STA (denoted as ZrSTA(*w*)) composites with polyoxometalate loadings (*w*) of about 2, 5, 10 and 20 wt% were prepared by using appropriate amount of 12-phosphotungstic and 12-silicotungstic acid, respectively. Mesoporous zirconia (*meso*-ZrO<sub>2</sub>) was also prepared following a procedure similar to that described above, without addition of heteropoly acids.

### Characterization

The X-ray diffraction (XRD) patterns were recorded on a PANalytical X'Pert Pro MPD X-ray diffractometer (45 kV and 40 mA) using Cu K $\alpha$  radiation ( $\lambda$ =1.5418 Å) in Bragg-Brentano geometry. Nitrogen adsorption and desorption isotherms were measured at 77 K using a NOVA 3200e volumetric analyzer (Quantachrome, USA). Before analysis, the samples were degassed at 150 °C under vacuum (<10<sup>-5</sup> Torr) for 12h to remove moisture. The specific surface areas

were calculated using the Brumauer-Emmett-Teller (BET) method<sup>20</sup> on the adsorption data in the 0.05–0.25 relative pressure ( $p/p_0$ ) range. The total pore volumes were derived from the adsorbed volume at  $p/p_0 = 0.95$ . The pore size distributions were determined by the NLDFT method<sup>21</sup> based on the adsorption data, using a data kernel for silica matrix with cylindrical pores. Micropore volume was estimated by the Dubinin-Radushkevich (DR) method in the low-pressure range  $p/p_0 = 0.0001$ –0.15. Transmission electron microscopy (TEM) was performed using a JEOL model JEM-2100 electron microscope equipped with an energy-dispersive X-ray spectroscopy (EDS) detector (Oxford Instruments) and operated at an accelerating voltage of 200 kV. Samples for TEM were prepared by suspending finely ground powder in ethanol using sonication, followed by depositing a drop of solution onto a Cu grid covered with carbon film. Infrared spectra were recorded on a Perkin Elmer Model Frontier FT-IR spectrometer. Spectra were obtained on averaging 100 interferograms with resolution of  $4\text{ cm}^{-1}$ . Samples were prepared as KBr pellets.

### Catalytic reactions

The catalytic oxidation of 1,1-diphenyl-2-methylpropene was carried out as follows. A mixture of substrate (0.1 mmol) and catalyst (0.5 mmol) was dissolved in 3 mL of ethanol into a 5 mL glass reactor with an open Teflon cap. The mixture was heated at  $50\text{ }^\circ\text{C}$  and the reaction was initiated by slowly adding (within a period of 3 min) the oxidant  $\text{H}_2\text{O}_2$  (3 equiv, 30% in  $\text{H}_2\text{O}$ ) into the ethanol solution. The assignment of products was realized by a combination of gas chromatography – mass spectrometry (Shimadzu GCMS-QP2010 Ultra) and  $^1\text{H}$  and  $^{13}\text{C}$  NMR spectroscopy (Bruker AMX 300 MHz) by withdrawing small aliquots from the reaction mixture. To establish the identity of the products unequivocally, the retention times and spectral data were compared to those of commercially available compounds. In all oxidations, the amount of POM in composite materials remains similar (about 2 mol%). As shown below, the sites located at or near the interface between the POM cluster and zirconia surface are the active species of the reaction and, therefore, mesoporous  $\text{ZrO}_2$ –POM composites act as catalysts and not as stoichiometric reagents.

## Results and discussion

### Structural characterization

X-ray diffraction (XRD) and transmission electron microscopy (TEM) experiments were performed to investigate the long-range order of the pore structure of  $\text{ZrP}(\text{TA})_w$  and  $\text{ZrSTA}(w)$  materials. As revealed by low-angle XRD (Fig. 1), the mesoporous zirconia ( $\text{meso-ZrO}_2$ ) and composite  $\text{ZrP}(\text{TA})_w$  and  $\text{ZrSTA}(w)$  samples show a relatively broad but well-defined diffraction peak at low  $2\theta$  scattering angles of  $1$ – $3^\circ$ , which according to transmission electron microscopy could be assigned to the (100) Bragg reflection of hexagonal  $p6mm$

structure. The low intensity of this diffraction peak for the composite samples with low loading amount of POMs (2 and 5 wt%) although suggests mesoscopic order, but with a small coherent domain size. On the basis of the pore symmetry and XRD data, it is possible to calculate the lattice constant ( $a_0$ ) of hexagonal motif from the d-spacing ( $a_0 = (2/\sqrt{3})d_{100}$ ) of the (100) diffraction. The results are given in Table 1.

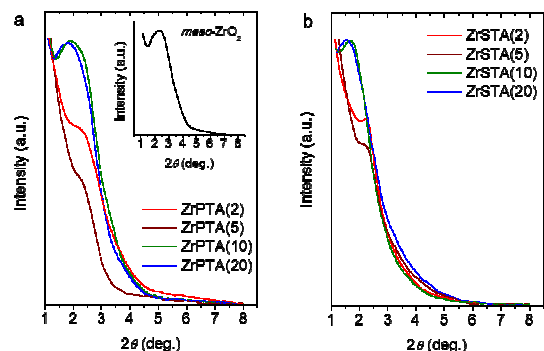


Fig. 1 Low-angle X-ray diffraction patterns of mesoporous (a)  $\text{ZrP}(\text{TA})_w$  and (b)  $\text{ZrSTA}(w)$  composite materials. The corresponding XRD pattern for mesoporous zirconia ( $\text{meso-ZrO}_2$ ) is given in inset of panel (a).

The wide-angle XRD patterns of the mesoporous  $\text{ZrP}(\text{TA})_w$  and  $\text{ZrSTA}(w)$  suggested the presence of nanocrystalline  $\text{ZrO}_2$ , as indicated from the broad reflections in the  $2\theta = 30$ – $60^\circ$  range (Fig. 2). The XRD peaks can be assigned to the (011), (110), (012), (112) and (121) Bragg reflections of the tetragonal phase of  $\text{ZrO}_2$  (JCPDS card no. 50-1089). As for the domain size of  $\text{ZrO}_2$  crystallites, it is difficult to estimate from the peak-width analysis of X-ray diffractions because of the low intensity of the peaks. However, their broadness obviously indicates crystallite size in the nanoscale range; typically below  $30\text{ nm}$ .<sup>22</sup> We did not observe any peak in the XRD patterns that could be assigned to the crystalline phase of  $\text{H}_3\text{PW}_{12}\text{O}_{40}$  and  $\text{H}_4\text{SiW}_{12}\text{O}_{40}$  compounds. This observation supports the notion that both PTA and STA heteropoly acids are homogeneously dispersed in mesoporous structures. However, given that the lower limit of detection of powder XRD is approximately 3–5 wt%, the presence of tiny amounts of nanometer-sized POM aggregates within the samples cannot be precluded.

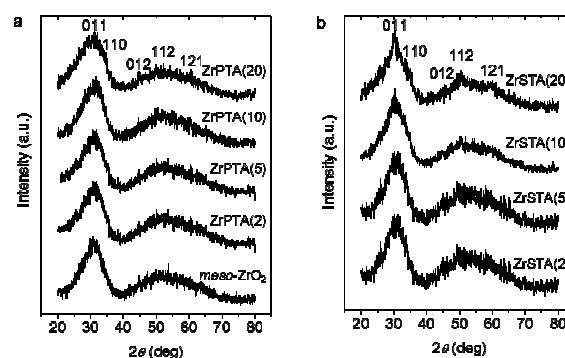
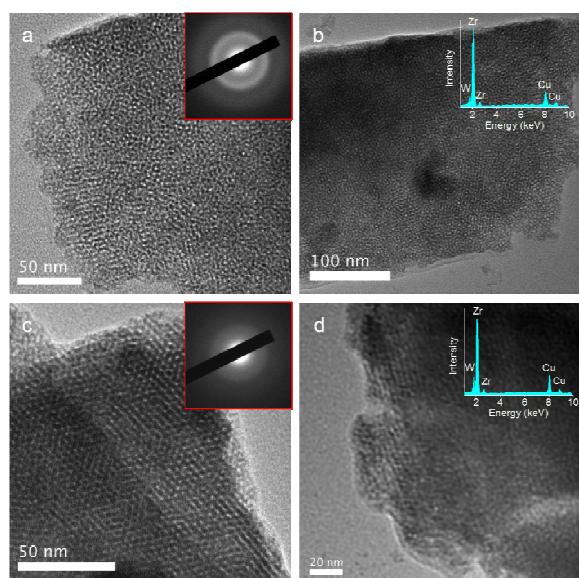
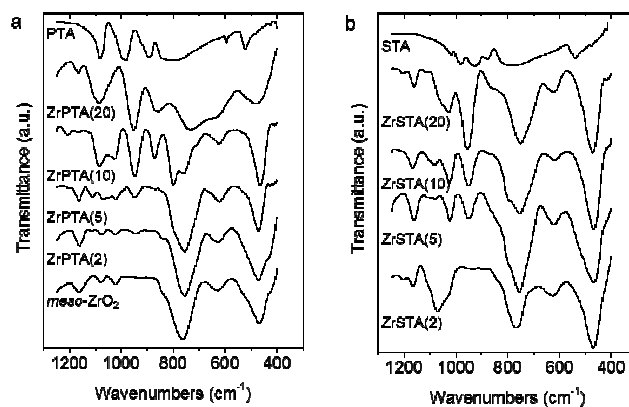


Fig. 2 Wide-angle XRD patterns of mesoporous (a)  $\text{ZrP}(\text{TA})_w$  and (b)  $\text{ZrSTA}(w)$  composite materials. The XRD pattern of mesoporous zirconia ( $\text{meso-ZrO}_2$ ) is also given in panel (a).

Direct examination of mesoporous ZrSTA(5) and ZrSTA(10) samples with TEM reveals extended mesoscopic pore ordering with uniform pores. As seen in Fig. 3, the ZrSTA(5) shows a poorly ordered, wormhole-like, pore structure with regular pores, while the ZrSTA(10) shows discernible domains of hexagonally arranged cylindrical pore channels, suggesting  $p6mm$  pore structure; although small deformations of the hexagonal honeycomb structure can be observed. Detailed analysis of TEM images indicated that both samples have an average pore-to-pore distance of  $\sim 5$  nm and pore diameter of  $\sim 2$  nm. This gives estimation for the framework wall thickness of about 3 nm, which is in good agreement with the results of the XRD and  $N_2$  porosimetry (see below). Furthermore, apart from XRD, the structure of crystalline phase was investigated by selected-area electron diffraction (SAED). SAED characterization suggests the poorly crystalline nature of zirconia, showing a broad and diffusive Debye-Scherrer diffraction ring (inset of Figs. 3a and 3c). According to the wide-angle XRD data, the electron diffraction ring could be tentatively assigned to the overlapped pair of (101) and (002) reflections of  $ZrO_2$  with tetragonal structure. Energy dispersive X-ray spectroscopy (EDS) acquired on TEM confirms the chemical composition of the as-prepared materials. As shown in Figs 3b and 3d (insets), the EDS spectra taken across a thin area of mesoporous structures indicate an average atomic ratio of Zr:W close to 97.3:2.7 and 94.8:5.2 for ZrSTA(5) and ZrSTA(10), respectively. In excellent agreement with the stoichiometry of reactions, these atomic ratios correspond to a weight percentage of STA content at  $\sim 5.3$  wt% for ZrSTA(5) and  $\sim 10.1$  wt% for ZrSTA(10). These results give evidence of the molecular dispersion and complete incorporation of heteropoly clusters into the mesoporous  $ZrO_2$  structure.



**Fig. 3** Representative TEM images and the corresponding SAED patterns (panel a and c, inset) taken along a thin area of the mesoporous (a and b) ZrSTA(5) and (c and d) ZrSTA(10) samples. The insets of panel b and d show the corresponding EDS spectra obtained on TEM. The copper peaks result from the TEM grid.



**Fig. 4** (a) Infrared spectra of mesoporous zirconia ( $meso-ZrO_2$ ) and ZrPTA( $w$ ) composite materials and 12-phosphotungstic acid (PTA) compound. (b) Infrared spectra of mesoporous ZrSTA( $w$ ) composites and 12-silicotungstic acid (STA) compound.

The Fourier transform-infrared (FT-IR) spectra of mesoporous ZrPTA( $w$ ) and ZrSTA( $w$ ) materials show a series of absorption peaks in the  $700\text{--}1100\text{ cm}^{-1}$  region that are similar to the spectra of pure heteropoly acids, *i.e.*  $H_3PW_{12}O_{40}$  and  $H_4SiW_{12}O_{40}$ . The IR spectra of high PTA-loaded ZrPTA( $w$ ) ( $w = 5, 10$  and  $20$  wt%) samples show the characteristic  $W=O_d$  and  $W-O_b-W$  (*i.e.*, between the corner-sharing  $WO_6$  octahedral) absorption bands of 12-phosphotungstic clusters at  $\sim 949\text{--}952$  and  $\sim 865\text{--}872\text{ cm}^{-1}$ , respectively, consistent with the presence of these clusters in composite materials (Fig. 4a).<sup>23</sup> These vibration bands are rather obscure on mesoporous ZrPTA(2) due to the low content (2 wt %) of PTA clusters. In comparison with the bulk PTA, the absorption peaks of  $W=O_d$  and  $W-O_b-W$  vibrations are remarkable red-shifted (by over  $30\text{ cm}^{-1}$ ), probably due to the strong conjugated interactions between the terminal ( $W=O_d$ ) and bridged ( $W-O_b-W$ ) oxygen atoms of  $(PW_{12}O_{40})^{3-}$  anions and zirconia matrix. The absorptions at  $\sim 1083$  and  $\sim 1026\text{ cm}^{-1}$  can be assigned as  $P-O_a$  stretching vibrational bands of the distorted  $PO_4$  central units in  $[PW_{12}O_{40}]^{3-}$  and lacunary  $[PW_{11}O_{39}]^{8-}$  Keggin clusters, respectively.<sup>24</sup> Given the relative strong basic character of zirconia surface, the formation of lacunary Keggin structures in these samples is a distinct possibility. Correspondently, the IR analysis of ZrSTA( $w$ ) showed absorption peaks at  $\sim 1024$ ,  $\sim 952$  and  $\sim 870\text{ cm}^{-1}$ , which are reasonably assigned to the  $Si-O_a$ ,  $W=O_d$  and  $W-O_b-W$  stretching vibrations of the  $[SiW_{12}O_{40}]^{4-}$  Keggin cluster, respectively (Fig. 4b).<sup>25</sup> The remarkable red shift of the  $W=O_d$  and  $W-O_b-W$  absorption bands (*ca.*  $15\text{--}30\text{ cm}^{-1}$ ) compared with those for pure STA, suggests that these clusters may also engages in strong interactions with the Zr-OH species through the  $W=O_d$  terminal and  $W-O_b-W$  bridging bonds. The strong absorptions at  $\sim 756\text{ cm}^{-1}$  and  $\sim 623\text{ cm}^{-1}$  are attributed to the stretching vibrations of Zr-O and Zr-O-Zr of tetragonal zirconia, respectively.<sup>26</sup>

The nanoporosity of the ZrPTA( $w$ ) and ZrSTA( $w$ ) heterostructures was determined by nitrogen physisorption measurements. As shown in Fig. 5, all samples display a combination of type I and type IV adsorption isotherms

associated with a distinct condensation step at relative pressure ( $p/p_0$ )  $\sim$  0.15–0.2, characteristic of mesoporous solids with uniform pores.<sup>27</sup> Analysis of the adsorption data with the Brunauer–Emmett–Teller (BET) method indicated large surface areas in the range of 126–229  $\text{m}^2\text{g}^{-1}$  and total pore volumes in range of 0.07–0.12  $\text{cm}^3\text{g}^{-1}$ . It can be observed that the surface area of these materials is strongly related to the POM loading and it increases as the POM fraction in the pore walls increases, see Table 1. This is quite peculiar considering the heavy elements of heteropoly acids (W, Mo) that composed the frameworks. It is worth noting that mesoporous  $\text{ZrO}_2$  exhibits a slightly lower BET surface area (118  $\text{m}^2\text{g}^{-1}$ ) and pore volume (0.06  $\text{cm}^3\text{g}^{-1}$ ), see ESI, Fig. +S1†. This signifies the role of heteropoly acids in self-assembly processes, in which the  $[\text{PW}_{12}\text{O}_{40}]^{3-}$  and  $[\text{SiW}_{12}\text{O}_{40}]^{4-}$  anions are possibly engaged in specific van der Waals and/or hydrogen bonding interactions with the surfactant micelles. Therefore, a  $\text{ZrO}_2$ –POM/surfactant composite phase can be stabilized, leading in self-assembly of these hybrid complexes into three-dimensional  $\text{ZrO}_2$ –POM mesostructures with long-range order. This assumption is also consistent with the structural deformation in low POM-loaded  $\text{ZrPTA}(w)$  and  $\text{ZrSTA}(w)$  ( $w = 2$  and 5 wt%) samples recommended by XRD and TEM results. To acquire more information of the porous structure of composite materials, the Dubinin–Radushkevich (DR) micropore analysis was applied in the low relative pressure region ( $p/p_0 < 0.15$ ). By means of this method, the micropore volume is estimated to be in range of 0.05–0.07  $\text{cm}^3\text{g}^{-1}$  that is coincided with a structural microporosity of about 50 to 60%. These data, along with the type-I shape of  $\text{N}_2$  adsorptions, readily confirm to the presence of interconnected pore network constructed from both mesopore and micropore channels. Table 1 summarizes all the textural parameters of mesoporous zirconia (*meso*- $\text{ZrO}_2$ ) and  $\text{ZrPTA}(w)$  and  $\text{ZrSTA}(w)$  composite materials.

**Table 1.** Textural properties of mesoporous zirconia (*meso*- $\text{ZrO}_2$ ) and  $\text{ZrPTA}(w)$  and  $\text{ZrSTA}(w)$  composite materials.

Sample	BET Surface ( $\text{m}^2\text{g}^{-1}$ )	Pore volume <sup>a</sup> ( $\text{cm}^3\text{g}^{-1}$ )	Pore size (nm)	Unit cell (nm)	WT <sup>b</sup> (nm)
<i>meso</i> - $\text{ZrO}_2$	118	0.06 (0.04)	2.5	4.3	1.8
$\text{ZrPTA}(2)$	126	0.07 (0.05)	2.4	4.5	2.1
$\text{ZrPTA}(5)$	160	0.07 (0.04)	2.3	4.6	2.3
$\text{ZrPTA}(10)$	207	0.09 (0.05)	2.3	5.1	2.8
$\text{ZrPTA}(20)$	210	0.09 (0.05)	2.3	5.6	3.3
$\text{ZrSTA}(2)$	140	0.08 (0.05)	2.5	4.7	2.2
$\text{ZrSTA}(5)$	155	0.08 (0.05)	2.6	5.1	2.5
$\text{ZrSTA}(10)$	229	0.11 (0.06)	2.6	5.8	3.2
$\text{ZrSTA}(20)$	218	0.12 (0.07)	2.6	6.2	3.6

<sup>a</sup>Cumulative pore volume at relative pressure  $p/p_0 = 0.95$ . In parenthesis: the micropore volume obtained by the DR plots. <sup>b</sup>The framework wall thickness given by  $\text{WT} = a_0 - D$ , where  $D$  is the pores size.

The pore size distribution calculated from the adsorption data based on the non-local density function theory (NLDFT) is quite narrow, indicating a uniform pore structure with an average pore diameter of  $\sim$ 2.2–2.6 nm. Since the mesoporous materials with different POM content show similar pore size, the continuous increase in unit cell size ( $a_0$ ) of  $\text{ZrPTA}(w)$  and  $\text{ZrSTA}(w)$  samples implies an relative increase of framework wall thickness. From a combination of NLDFT pore sizes and XRD lattice constants, we obtained a pore wall thickness from 2.1 to 3.3 nm for  $\text{ZrPTA}(w)$  and from 2.2 to 3.6 nm for  $\text{ZrSTA}(w)$ . Based on similar calculations, the framework wall thickness of mesoporous zirconia (*meso*- $\text{ZrO}_2$ ) was estimated to be *ca.* 1.8 nm. The increase of the wall thickness with subsequent increase of the POM loading is consistent with the integration of these heteropoly acids into the framework of composite materials. This is in agreement with the XRD and TEM-EDS data.

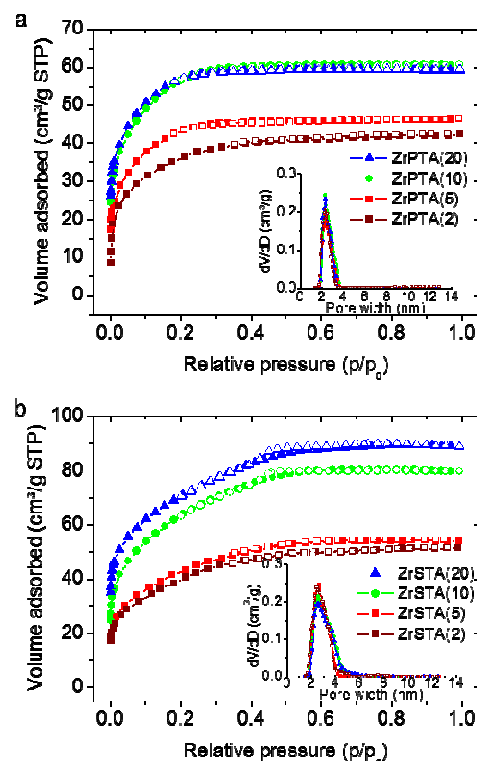
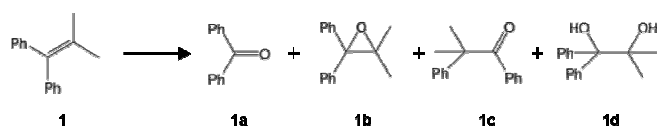


**Fig. 5**  $\text{N}_2$  adsorption–desorption isotherms at 77K for mesoporous  $\text{ZrPTA}(w)$  and  $\text{ZrSTA}(w)$  materials. Insets: the corresponding NLDFT pore size distributions.

### Catalytic Oxidation

The catalytic activity of mesoporous  $\text{ZrPTA}(w)$  and  $\text{ZrSTA}(w)$  composites was evaluated in oxidation of 1,1-diphenyl-2-methylpropene (**1**) as a test reaction<sup>19</sup>, using hydrogen peroxide as the oxidant (Scheme 1). The selective oxidation of alkene (**1**) under mild conditions is a challenging issue in synthesis of organic fine chemicals.<sup>28</sup> All reactions were performed in ethanol that gave the best results in terms of catalytic activity. The optimized reaction

conditions was obtained by using ZrSTA(5) catalyst for the oxidation of **1** in different media. As seen in supporting Fig. S2†, the conversion of **1** can be improved when the reaction performed in ethanol (>99%), while oxidation of **1** in other solvents such as methanol and acetonitrile although proceeded fast, but in lower conversion yields (*i.e.* 93% and 87%, respectively). Notably, the reaction proceeds at a negligible rate (<2% conversion) in toluene, probably due to the low solubility of H<sub>2</sub>O<sub>2</sub> and hydrophilic character of the catalyst.



**Scheme 1.** Oxidation of **1** over mesoporous ZrPTA(w) and ZrSTA(w) composite catalysts.

Next, efforts were directed to investigate the catalytic performance of composite catalysts featuring different POM loading. The oxidations of **1** using hydrogen peroxide as oxidant was monitored by GC-MS analysis and the results are shown in Fig. 6 and Fig. S3 of the ESI†. It is evident that the catalytic activity for both ZrPTA(w) and ZrSTA(w) composites is strongly related to the amount of the incorporated POM clusters. Namely, the 2–5 wt% POM-loaded samples showed a moderate-to-high conversion of **1**, while composite materials containing large amount of heteropoly acids (10–20 wt%) exhibited a dramatic drop in conversion yield. It is noteworthy that employing pure mesoporous zirconia and heteropoly acids as catalysts gave poor activity under similar reaction conditions (~25% and less than 2% in 30 min, respectively). Based on the **1** consumption, the ZrSTA(5) catalyst achieves the highest activity, giving >99% conversion of oxidative products in only 30 min. Meanwhile, control experiment showed that in the absence of catalyst no reaction takes places. The present data suggest that, apart to the surface area, the elemental PTA/ZrO<sub>2</sub> and STA/ZrO<sub>2</sub> composition has a profound influence on the catalytic oxidation processes. It seems that ZrSTA(w) and ZrPTA(w) are really synergistic catalysts, wherein Keggin anions and Zr(IV) oxohydroxide (ZrO<sub>x</sub>(OH)<sub>y</sub>) species potentially act as cooperative catalytic sites for the activation of C=C bonds of **1** substrate. This is a different from the case of pure ZrO<sub>2</sub> and heteropolytungstic acids.

Table 2 summarizes the results of the catalytic oxidation of **1** on heterogeneous ZrPTA(w) and ZrSTA(w) as well as homogeneous PTA and STA catalysts. In all cases the corresponding epoxide **1b** and ketone **1c** were formed as major oxidative products, accompanying with small amount of the ketone **1a** and diol **1d**. Benzophenone **1a** is a cleavage product of the corresponding 1,2-dioxitane alkene, which is a non stable intermediate.<sup>19</sup> While, a notable amount of ketone **1c** should be formed through 1,2-phenyl shift<sup>29</sup> of the corresponding diol **1d**, as verified by GC-MS and H<sup>1</sup> NMR measurements,<sup>30</sup> as well as by control catalytic experiments<sup>31</sup>. As seen in Table 2, all the ZrPTA(w) and ZrSTA(w) catalysts promote the oxidation of **1**

alkene with moderate-to-good chemoselectivity (36–58%) for **1c**.

**Table 2.** Selective oxidation of **1** with H<sub>2</sub>O<sub>2</sub> catalyzed by mesoporous zirconia (*meso*-ZrO<sub>2</sub>) and ZrPTA(w) and ZrSTA(w) composites as well as homogeneous PTA and STA compounds.<sup>a</sup>

Catalyst	Conversion <sup>b</sup> (%)	Relative yield <sup>c</sup> ( <b>1a</b> : <b>1b</b> : <b>1c</b> : <b>1d</b> )	Kinetic constant ( <i>k</i> ) <sup>d</sup> (h <sup>-1</sup> )
<i>meso</i> -ZrO <sub>2</sub>	25	10:15:59:16	0.010
ZrPTA(2)	78	6:13:58:23	0.048
ZrPTA(5)	87	6:29:41:24	0.064
ZrPTA(10)	38	7:32:37:24	0.012
ZrPTA(20)	5	12:32:36:20	0.001
PTA	<1		
ZrSTA(2)	65	6:14:56:24	0.041
ZrSTA(5)	>99	8:14:48:30	0.168
ZrSTA(10)	40	6:25:48:21	0.017
ZrSTA(20)	8	12:25:41:22	0.003
STA	<2		

<sup>a</sup>Reaction conditions: 0.1 mmol of **1**, 0.5 mmol of catalyst, 0.3 mmol of H<sub>2</sub>O<sub>2</sub> (30 wt.% in water), 3 ml ethanol, 50 °C, 30 min. <sup>b</sup>Based on the consumption of alkene **1** measured by GC. <sup>c</sup>Products relative yield determined by GC-MS using nonane as internal standard.

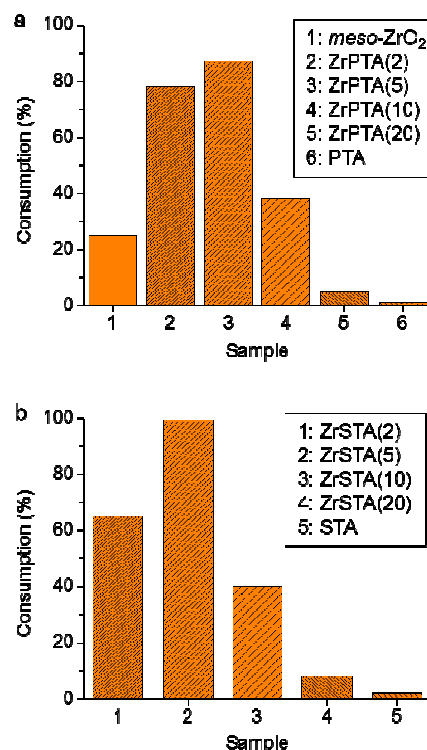


**Fig. 6** Oxidation of **1** catalyzed by heterogeneous mesoporous ZrO<sub>2</sub> (*meso*-ZrO<sub>2</sub>), ZrPTA(w) and ZrSTA(w) materials and homogeneous PTA (H<sub>3</sub>PW<sub>12</sub>O<sub>40</sub>) and STA (H<sub>4</sub>SiW<sub>12</sub>O<sub>40</sub>) compounds. *Experimental conditions:* 0.1 mmol **1**, 0.5 mmol catalyst, 3 equiv. H<sub>2</sub>O<sub>2</sub> (30% in water), 3 mL ethanol, 50 °C, 30 min.

The time evolution of **1** conversion can be reasonably accounted by a pseudo-first order reaction model. This is reasonable if we account the excess of H<sub>2</sub>O<sub>2</sub>, so that its concentration could be considered constant during the reaction. The Fig. 7 shows the plots of ln(C<sub>t</sub>/C<sub>0</sub>) (where, C<sub>0</sub> is the concentrations of **1** at the initial state of reaction and C<sub>t</sub> is the concentration at the time t) as a function of time, by which the

reaction rate constants ( $k$ ) as a slope of the linear fits were obtained. The corresponding  $k$  values, shown in Table 2, indicate higher reaction rate on ZrSTA(5) compared to the other catalysts, despite the less ordered mesostructure and relative low surface area. Notably, the catalytic oxidation rate over ZrSTA(5) is about 17 times greater than mesoporous  $\text{ZrO}_2$  sample ( $0.168 \text{ h}^{-1}$  vs.  $0.010 \text{ h}^{-1}$ ) under similar conditions. The enhancement of catalytic activity over ZrSTA(5) can be regarded as a result of synergistic interactions between the  $[\text{SiW}_{12}\text{O}_{40}]^{4-}$  anions and  $\text{ZrO}_2$  matrix, as previously discussed. Nevertheless, the well dispersion of POM units and the open-framework structure are important virtues, which may also account for the high reactivity of these materials.

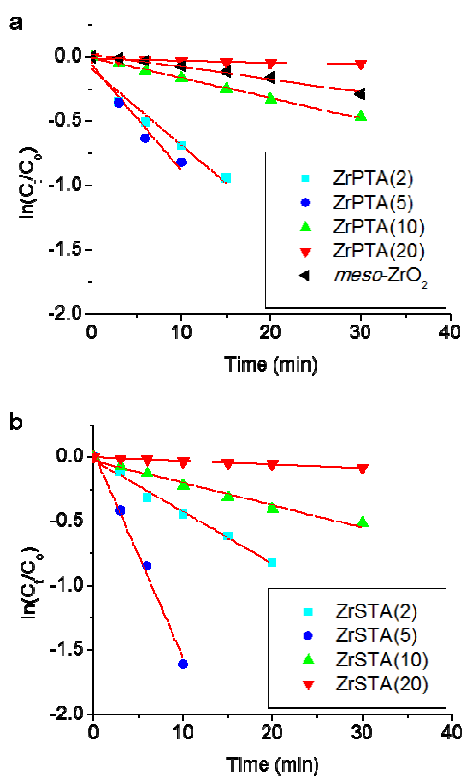


**Fig. 7** Kinetic analysis of the 1,1-diphenyl-2-methylpropene oxidation over heterogeneous mesoporous zirconia ( $\text{meso-ZrO}_2$ ),  $\text{ZrPTA}(w)$  and  $\text{ZrSTA}(w)$  and homogeneous PTA ( $\text{H}_3\text{PW}_{12}\text{O}_{40}$ ) and STA ( $\text{H}_4\text{SiW}_{12}\text{O}_{40}$ ) compounds. The corresponding red lines are fit to the data.

The  $\text{ZrPTA}(5)$  catalyst is stable and it can be reused for the next catalytic run without significant loss in catalytic activity. After catalysis, the solid  $\text{ZrPTA}(5)$  was separated from the reaction mixture by filtration, washed with fresh ethanol several times and dried at ambient conditions, and used for the next catalytic cycle. The results in Fig. S4 of the ESI<sup>†</sup>, show that the consumption of **1** remains as high as  $\sim 96\%$  and  $\sim 99\%$  after 30 min and 2 h reaction time, respectively, *i.e.* very close to the conversion levels achieved by the fresh catalyst. Nitrogen physisorption measurements on reused sample gave no signs of decomposition of mesostructure, indicating surface area of  $149 \text{ m}^2\text{g}^{-1}$  and total pore volume of  $0.08 \text{ cm}^3\text{g}^{-1}$  (Fig. S5). Moreover, elemental EDS microanalysis and IR spectroscopy showed no

change in the chemical composition and Keggin structure of the incorporated  $[\text{SiW}_{12}\text{O}_{40}]^{4-}$  clusters of reused sample, thereby, confirming high durability of recyclability. In particular, the EDS spectra showed an average Zr/W atomic ratio of  $\sim 97.3:2.7$ , which corresponds to a STA content of  $\sim 5.1 \text{ wt}\%$ , in accordance with the nominal composition of the as-prepared catalyst, see ESI, Fig. S6<sup>†</sup>. The IR spectrum displayed the characteristic Si–O<sub>a</sub>, W=O<sub>d</sub> and W–O<sub>b</sub>–W vibration bands at  $\sim 1024$ ,  $\sim 941$  and  $\sim 882 \text{ cm}^{-1}$  respectively, reflecting the Keggin structure of the 12-silicotungstic acids (Fig. S7 of the ESI<sup>†</sup>). Nevertheless, minimal decomposition or leaching of incorporated STA clusters (on the basis of EDS and IR analysis limitations) by the excess of  $\text{H}_2\text{O}_2$  cannot be excluded.<sup>32</sup>

## Conclusions

We have successfully prepared a series of mesoporous composite frameworks consisting of zirconium oxide ( $\text{ZrO}_2$ ) and 12-phosphotungstic (PTA) or 12-silicotungstic (STA) acid compounds through a surfactant-templating approach. The as-prepared materials possess  $\text{ZrO}_2$ –PTA and  $\text{ZrO}_2$ –STA framework composition with different POM loadings, *i.e.* ranging from 2 to 20 wt%. Characterization by TEM and  $\text{N}_2$  physisorption showed a mesoporous structure with large internal surface area ( $126$ – $229 \text{ m}^2\text{g}^{-1}$ ) and narrow-sized mesopores (*ca.* 2.2–2.6 nm). Moreover, XRD, EDS and IR measurements indicated that the Keggin structure of the incorporated clusters was preserved intact into the mesoporous frameworks, forming rather a solid solution with the  $\text{ZrO}_2$  species. Although  $\text{ZrO}_2$  and heteropoly acids alone have little catalytic activity,  $\text{ZrPTA}(w)$  and  $\text{ZrSTA}(w)$  composites exhibit excellent activity in 1,1-diphenyl-2-methylpropene oxidation, using hydrogen peroxide as oxidant. Unlike the specific surface area, the framework composition of these materials has a dominant effect on the catalytic performance, indicating higher catalytic activity for  $\text{ZrSTA}(w)$  composite sample loaded with 5 wt% of STA clusters. Remarkably, the  $\text{ZrSTA}(5)$  showed much higher activity than mesoporous zirconia and 12-silicotungstic acids alone, which is reflected in the about 17-fold increase of the conversion rate compared to mesoporous  $\text{ZrO}_2$ ; the homogeneous STA catalyst showed negligible catalytic activity under similar conditions. Furthermore, the  $\text{ZrSTA}(5)$  composite demonstrated very good durability and recyclability without decomposition of STA clusters and degradation of mesostructure. These results suggest that these complex materials should have great application potential in oxidation catalysis, including size-selective oxidation of alkenes.

## Acknowledgements

Financial support by the Greek Ministry of Education under Excellence grant (ARISTEIA-2691) and THALES project (MIS 377064) are kindly acknowledged.

## Notes and references

<sup>a</sup> Department of Materials Science and Technology, University of Crete, Voutes 71003, Heraklion, Greece. E-mail: garmatas@materials.uoc.gr

- <sup>b</sup> Department of Chemistry, Aristotle University of Thessaloniki, University Campus 54124, Thessaloniki, Greece.
- † Electronic Supplementary Information (ESI) available: N<sub>2</sub> physisorption data for *meso*-ZrO<sub>2</sub>, catalytic data for ZrSTA(5) in different media, time evolution profiles of **1** oxidation over *meso*-ZrO<sub>2</sub>, ZrPTA(*w*) and ZrSTA(*w*) materials and PTA and STA compounds, and catalytic data, N<sub>2</sub> adsorption-desorption isotherms and EDS and IR spectra of reused ZrSTA(5) catalyst. See DOI: 10.1039/b000000x/
- 1 I.V. Kozhevnikov, *Catalysis by Polyoxometalates*, Wiley, Chichester, England, 2002.
  - 2 M.V. Vasylyev and R. Neumann, *J. Am. Chem. Soc.*, 2004, **126**, 884.
  - 3 Y. Nishiyama, Y. Nakaqawa and N. Mizuno, *Angew. Chem. Int. Ed.*, 2001, **40**, 3639; R. Neumann and M. Gara, *J. Am. Chem. Soc.*, 1995, **117**, 5066.
  - 4 C.F. Oliveira, L.M. Dezaneti, F.A.C. Garcia, J.L. de Macedo, J.A. Dias, S.C.L. Dias and K.S.P. Alvim, *Appl. Catal. A: Gen.*, 2010, **372**, 153; C.L. Hill, *Chem. Rev.*, 1998, **98**, 1; C.L. Hill, and C.M. Prosser-McCartha, *Coord. Chem. Rev.*, 1995, **143**, 407.
  - 5 S. Uchida, M. Hashimoto and N. Mizuno, *Angew. Chem. Int. Ed.*, 2002, **41**, 2814; K. Zhu, J. Hu, X. She, J. Liu, Z. Nie, Y. Wang, C.H.F. Peden and J.H. Kwak, *J. Am. Chem. Soc.*, 2009, **131**, 9715; K. Inumaru, T. Ishihara, Y. Kamiya, T. Okuhara and S. Yamanaka, *Angew. Chem. Int. Ed.*, 2007, **46**, 7625.
  - 6 S.L. Suib, *New and future developments in catalysis: Hybrid materials, composites, and organocatalysts*, Elsevier, Amsterdam, 2013.
  - 7 G.S. Armatas, A.P. Katsoulidis, D.E. Petrakis, P.J. Pomonis and M.G. Kanatzidis, *Chem. Mater.*, 2010, **22**, 5739.
  - 8 A. Lapkin, B. Bozkaya, T. Mays, L. Borello, K. Edler and B. Crittenden, *Catal. Today*, 2003, **81**, 611.
  - 9 L.R. Pizzio, C.V. Caceres and M.N. Blanco, *Appl. Catal. A: Gen.*, 1998, **167**, 283.
  - 10 X. Qu, Y. Guo and C. Hu, *J. Mol. Catal. A: Gen.*, 2007, **262**, 128.
  - 11 S. Hodjati, K. Vaezzadeh, C. Petit, V. Pitchon and A. Kienemann, *Top. Catal.*, 2001, **16**; L.R. Pizzio, P.G. Vazquez, C.V. Caceres and M.N. Blanco, *Appl. Catal. A: Gen.*, 2003, **256**, 125.
  - 12 P. Vazquez, L. Pizzio, G. Romanelli, J. Autino, C. Caceres and M. Blanco, *Appl. Catal. A: Gen.*, 2002, **235**, 233.
  - 13 I. Tamiolakis, I.N. Lykakis, A.P. Katsoulidis, M. Stratakis and G.S. Armatas, *Chem. Mater.*, 2011, **23**, 4204.
  - 14 Y. Guo, K. Li and J.H. Clark, *Green Chem.*, 2007, **9**, 839; M. Vazylyev and R. Neumann, *J. Am. Chem. Soc.*, 2004, **126**, 884; I. Tamiolakis, I.N. Lykakis, A.P. Katsoulidis, C.D. Malliakas and G.S. Armatas, *J. Mater. Chem.*, 2012, **22**, 6919.
  - 15 V. Dufaud, F. Lefebvre, G.P. Niccolai and M. Aouine, *J. Mater. Chem.*, 2009, **19**, 1142; Y. Guo, K. Li and J.H. Clark, *Green Chem.*, 2007, **9**, 839; R. Zhang and C. Yang, *J. Mater. Chem.*, 2008, **18**, 2691.
  - 16 R. Neumann and I.J. Assael, *J. Chem. Soc. Chem. Commun.*, 1989, 547; X. Lin, Y. Wang and L. Wu, *Langmuir*, 2009, **25**, 6081.
  - 17 J. Kaspar, P. Fornasiero and N. Hickey, *Catal. Today*, 2003, **77**, 419.
  - 18 G.S. Armatas, G. Bilis and M. Louloudi, *J. Mater. Chem.*, 2011, **21**, 2997.
  - 19 Y. Sawaki and C.S. Foote, *J. Org. Chem.*, 1983, **48**, 4934; I.N. Lykakis, G.C. Vougioukoulakis and M. Orfanopoulos, *J. Org. Chem.*, 2006, **71**, 8740.
  - 20 S. Brunauer, L.S. Deming, W.S. Deming and E. Teller, *J. Am. Chem. Soc.*, 1940, **62**, 1723.
  - 21 P.I. Ravikovitch, D. Wei, W.T. Chueh, G.L. Haller and A.V. Neimark, *J. Phys. Chem. B*, 1997, **101**, 3671.
  - 22 S. Shukla and S. Seal, *J. Phys. Chem. B*, 2004, **108**, 3395
  - 23 C. Rocchicciolo-Deltcheff, M. Gournier, R. Franck and R. Thouvenot, *Inorg. Chem.*, 1983, **22**, 207.
  - 24 E. Lopez-Salinas, J.G. Hernandez-Cortez, I. Schifter, E. Torres-Garcia, J. Navarrete, A. Gutierrez-Carrillo, T. Lopez, P.P. Lottici and D. Bersani, *Appl. Catal. A*, 2000, **193**, 215; R.D. Peacock and T.J.R. Weakley, *J. Chem. Soc.*, 1971, 1836.
  - 25 C. Rocchicciolo-Deltcheff, R. Thouvenot and R. Franck, *Spectrochimica Acta*, 1976, **32A**, 587.
  - 26 K. Nakamoto, *Infrared and Raman Spectra of Inorganic and Coordination Compounds*, 4th ed., Wiley, New York, 1986; E. Lopez-Salinas, J.G. Hernandez-Cortez, I. Schifter, E. Torres-Garcia and T. Lopez, *Appl. Catal. A*, 2000, **193**, 215.
  - 27 S.J. Gregg and K.S.W. Sing, *Adsorption, Surface Area and Porosity*, Academic Press, New York, 1982.
  - 28 M. Stratakis and M. Orfanopoulos, *Tetrahedron*, 2000, **56**, 1565; N. Mizuno, K. Yamaguchi and K. Kamata, *Coord. Chem. Rev.*, 2005, **249**, 1944.
  - 29 M. Jiang, L. -P. Liu and M. Shi, *Tetrahedron*, 2007, **63**, 9599; R. Akaba, S. Aihara, H. Sakuragi and K. Tokumaru, *Bull. Chem. Soc. Jpn.*, 1991, **64**, 1419; W. Y. Suprum, *J. Prakt. Chem.*, 1998, **340**, 247.
  - 30 U. Scheffler and R. Mahrwald, *Helv. Chim. Acta*, 2012, **95**, 1970; R. E. Lyle and G. G. Lyle, *J. Org. Chem.* 1953, 1058.
  - 31 Control experiment was realized as following: First, we performed the catalytic reaction using 0.1 mmol of **1**, 0.5 mmol of ZrSTA(5) catalyst (containing 2 mol% STA) and 3 eq. H<sub>2</sub>O<sub>2</sub> (30% in water) in 3 mL ethanol for 20 min. After this, the reaction mixture was filtrated over a Celite-silica pad to remove H<sub>2</sub>O<sub>2</sub>. The filtrate (containing the oxidative products **1a**, **1b**, **1c** and **1d**), was then subject to reaction at 50 °C for another 2h (with the addition of 0.5 mmol of catalyst) and the product ratios were analyzed by GC-MS. No significant changes were observed for the amounts of **1a** and **1b**, while an increase of the **1c/1d** product yield ratio from 1.7 to 3.2 was obtained.
  - 32 L. Salles, C. Aubry, R. Thouvenot, F. Robert, C Dorémieux-Morin, G. Chottard, H. Ledon, Y. Jeannin and J.-M. Brégeault, *Inorg. Chem.*, 1994, **33**, 871; L. Salles, J.-Y. Piquemal, R. Thouvenot, C. Minot and J.-M. Brégeault, *J. Mol. Catal. A: Chem.*, 1997, **117**, 375.

## Table of contents

Ordered mesoporous composite materials consisting of nanocrystalline  $\text{ZrO}_2$  and 12-phosphotungstic and 12-silicotungstic acids were synthesized and shown to be superior catalysts than individual components.

